

Table of Contents

Figure S1. Precision, recall, and F1 scores for SNV and indel calls for ONT and Illumina small variant calls using PacBio assemblies as the truth set.	2
Figure S2. Precision, recall, and F1 scores for SNV and indel calls for ONT small variant calls from both the Napu (PMDV) and alignment (Clair3) pipelines using Illumina data as the truth set.	3
Figure S3. Percent of genome assembled by Flye and Shasta-Hapdup.	4
Figure S4. IGV screenshots of chromosome 7 assemblies.	5
Figure S5. Pangenome principal component analysis.	7
Figure S6. Evaluation of L1HS elements in the first 100 assemblies.	9
Figure S7. Evaluation of per-sample insertions and deletions by type, chromosome, and SV caller	10
Figure S8. Distribution of SV events genome-wide, all populations	11
Figure S9. Concordance of SVs by caller and evaluation of joint SV calls.	12
Figure S10. Example of false positive SVs called only by hapdiff.	13
Figure S11. Evaluating the functional impact of structural variants.	14
Figure S12. Evaluation of SVs in exons of medically relevant genes	15
Figure S13. IGV view of a previously described deletion that includes HBM, HBA2, HBA1, HBQ1	16
Figure S14. Evaluation of X-linked SVs in 46,XY individuals	17
Figure S15. Phased IGV screenshot depicting long-read alignments involving two pharmacogene hybrid star alleles. ...	18
Figure S16. Repeat expansion plots for 66 disease-associated loci.	19
Figure S17. IGV screenshots of repeat expansions in RFC1 observed in 5 samples.	20
Figure S18. IGV screenshots of ATXN10 repeat expansions	23
Figure S19. IGV screenshots of repeat expansion within FGF14	25
Figure S20. Principal component analysis using methylation.	26
Figure S21. Evaluating methylation differences at SNURF-SNRPN.	27
Figure S22. Output from MeOW showing DMRs within 3 samples that have 10 or more DMRs.	28
Figure S23. Unique DMRs are associated with nearby changes in gene expression.	32

Figure S1. Precision, recall, and F1 scores for SNV and indel calls for ONT and Illumina small variant calls using PacBio assemblies as the truth set.

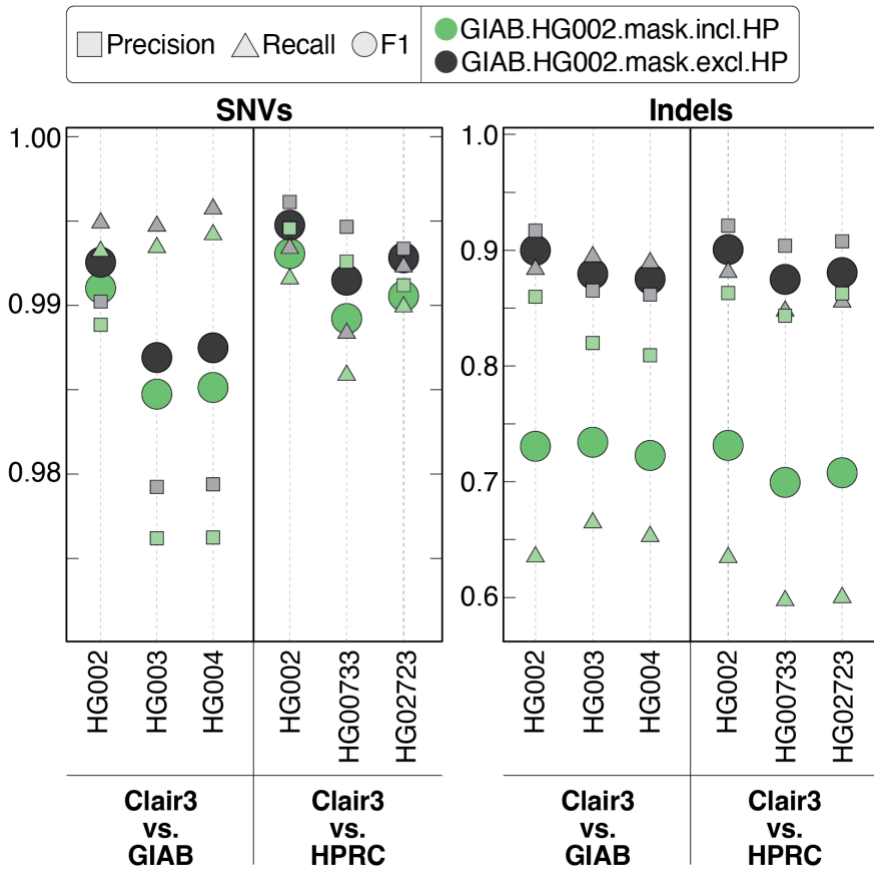


Figure S2. Precision, recall, and F1 scores for SNV and indel calls for ONT small variant calls from both the Napu (PMDV) and alignment (Clair3) pipelines using Illumina data as the truth set.

Variants called using PMDV are shown without masking (A), results that include masking can be found in the main text. Variants called by Clair3 are shown genome-wide (B), in GIAB high-confidence regions only (C), and in GIAB high-confidence regions excluding homopolymers 4 nucleotides or greater +/- one nucleotide on either side (D).

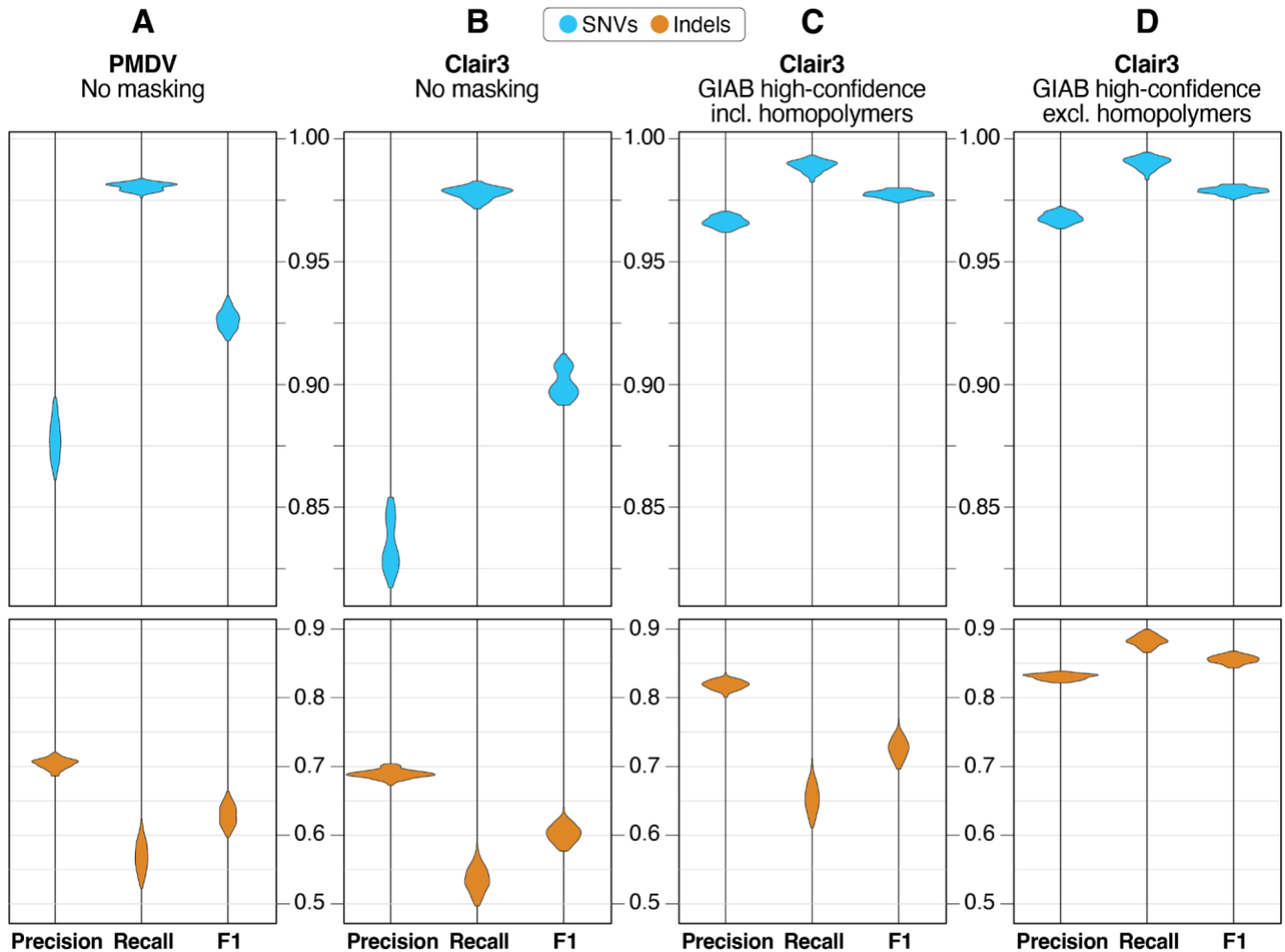


Figure S3. Percent of genome assembled by Flye and Shasta-Hapdup.

Violin plot showing the percentage of genome assembled for each sample by Flye and Shasta-Hapdup. The x-axis represents the assembler and the y-axis represents the percentage of GRCh38 reference genome covered by contigs for each assembly. The median values for Flye and Shasta-Hapdup assemblies for all 100 samples are 93.6% and 93.5%, respectively.

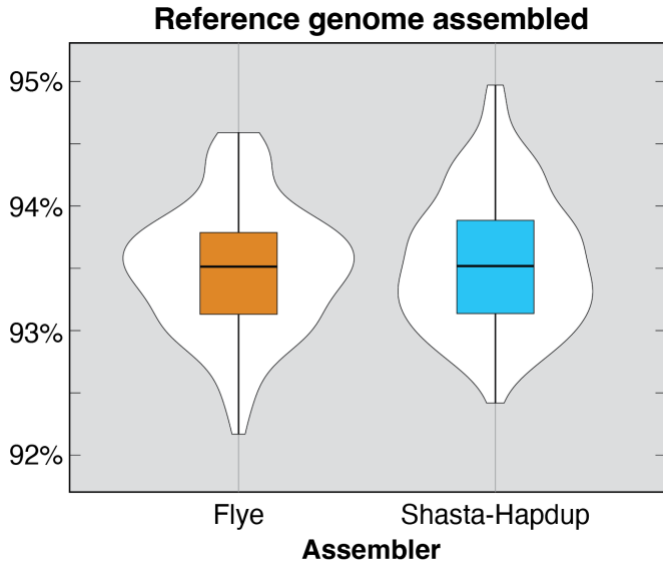
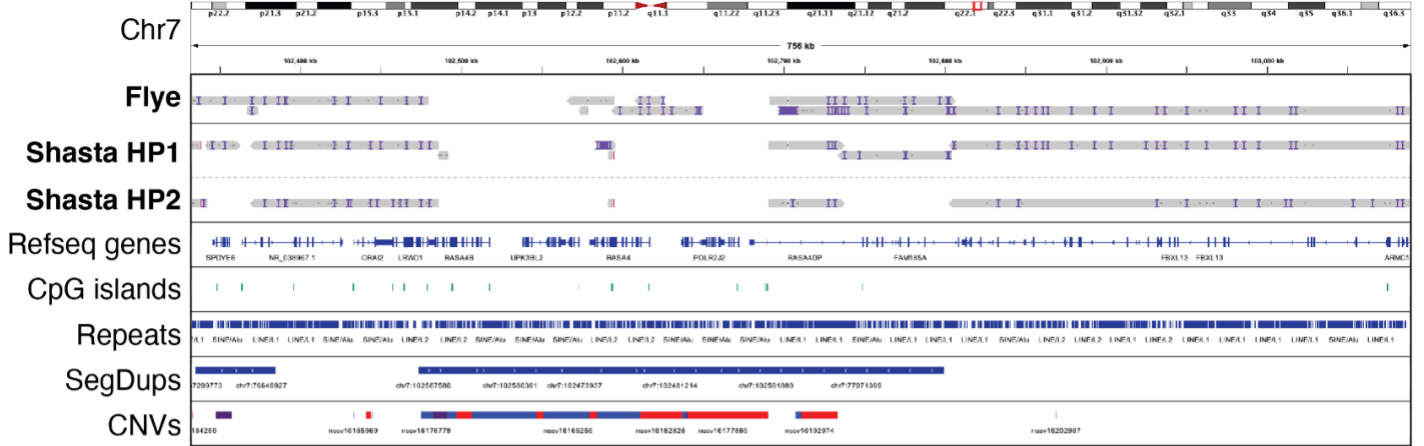


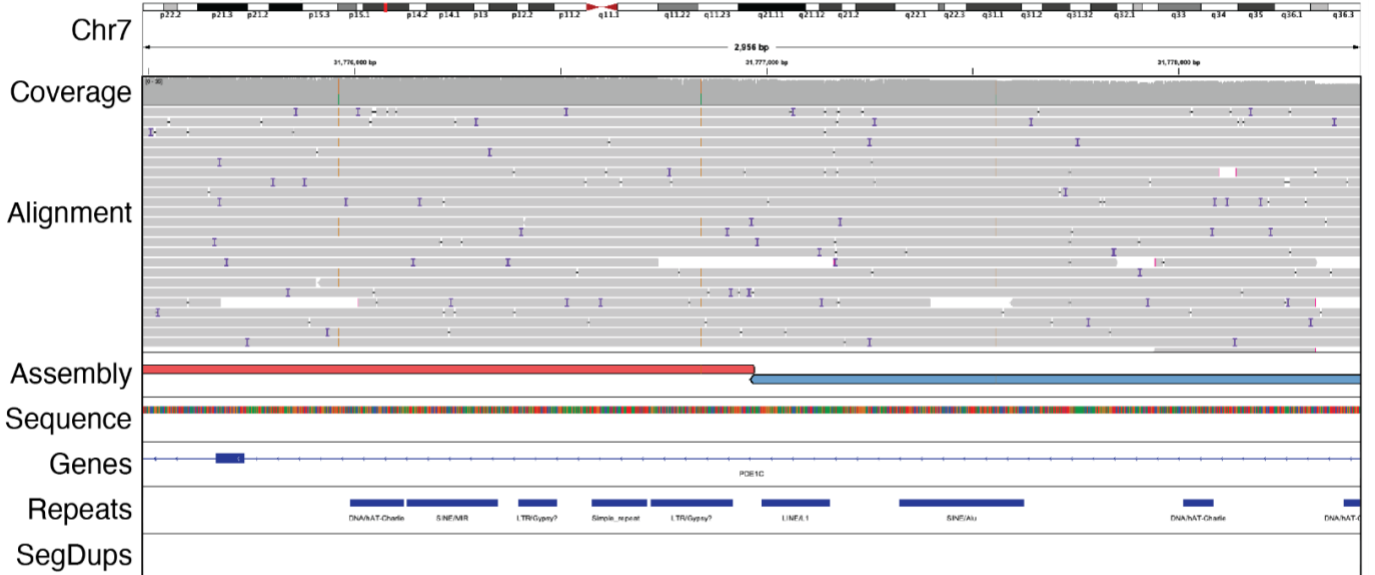
Figure S4. IGV screenshots of chromosome 7 assemblies (*see next page*).

A. Example of a location where the presence of a segmental duplication is associated with breaks in assemblies in both Flye and Shasta-Hapdup for HG02373. **B.** Example of a region with a discontinuity in the Flye assembly contigs in GM19035. This break occurs in a region outside of a segmental duplication or a satellite repeat. The alignment and coverage tracks at the top suggest no aberrations or increased coverage that could indicate increased likelihood of an assembly break. IGV view is approximately 2,900 bp. **C.** Example of a position where Shasta-Hapdup assembled contigs break in both haplotype-resolved assemblies in HG01801. This break occurs in a region outside of a segmental duplication or satellite repeat. The alignment and coverage tracks at the top suggest no aberrations or increased coverage that could indicate increased likelihood of assembly breaks. IGV view is approximately 23 kbp.

A HG02373 | Flye and Shasta-Hapdup



B GM19035 | Flye



C HG1801 | Shasta-Hapdup

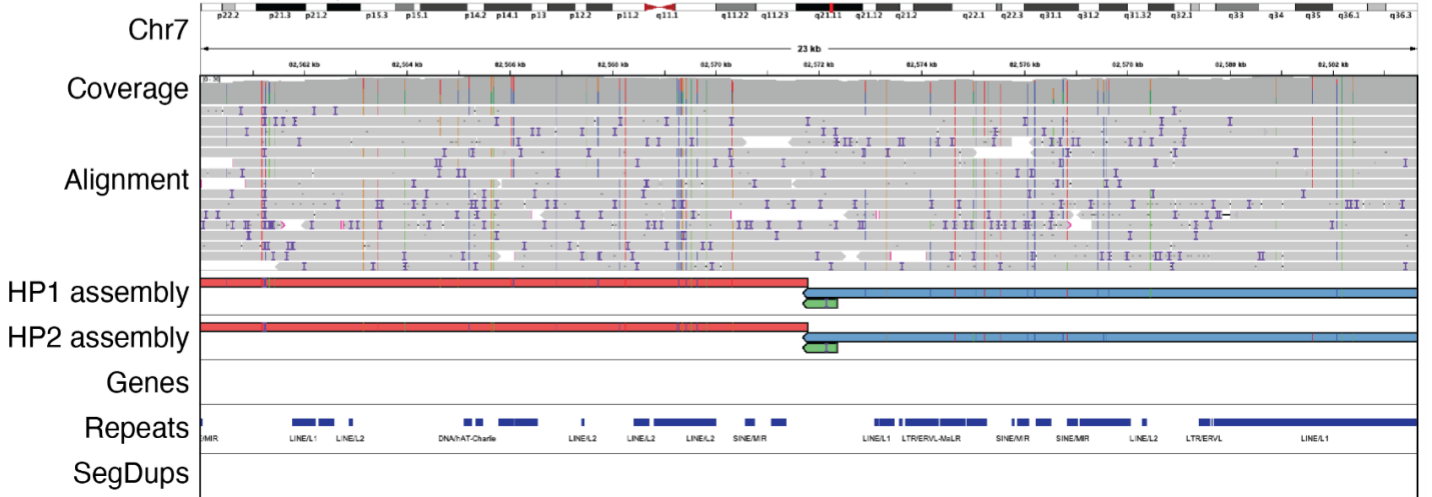


Figure S5. Pangenome principal component analysis (*see next page*).

A. Graph-based principal component analysis of chromosome 20 assemblies – including 100 Shasta-Hapdup samples, 44 HPRC samples, and the GRCh38, CHM13 (v2.0), and HG002 (v1.0.1) human reference genomes – revealed clear separation along the first principal component (PC1). The two clusters correspond to the HPRCy1 assemblies (right) and 100 Shasta-Hapdup assemblies (left). Because our assemblies cluster close to GRCh38, whose centromeric sequences were masked, we interpreted PC1 as representing centromeric diversity of the assemblies. Experience with ONT based assemblies suggests that the ONT-only assemblies are currently less able to assemble highly repetitive sequences compared to those which include HiFi data. **B.** Graph-based principal component analysis of euchromatic, non-centromeric fraction of the chromosome 20 assemblies—including 100 Shasta-Hapdup samples, 44 HPRC samples, and the GRCh38, CHM13 (v2.0), and HG002 (v1.0.1) human reference genomes—revealed no distinct separation between the Shasta-Hapdup and HPRC samples. The 4 reference genomes cluster because their entire sequence is considered, including the heterochromatic regions. Data points were visually distinguished by color and shape according to their group. In general, our assemblies are slightly more spread in both PC1 and PC2, which possibly relates to higher base-level error rates in the ONT-only assemblies.

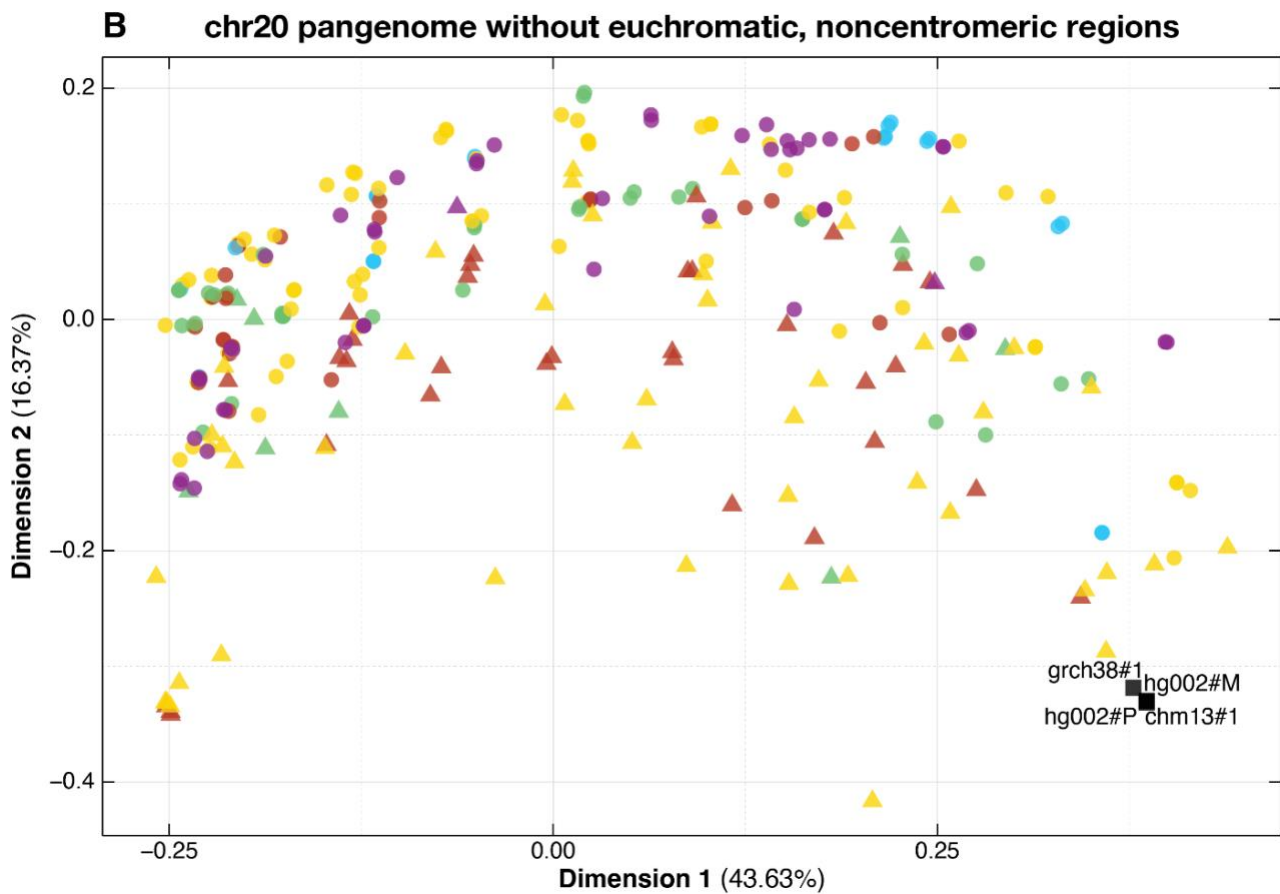
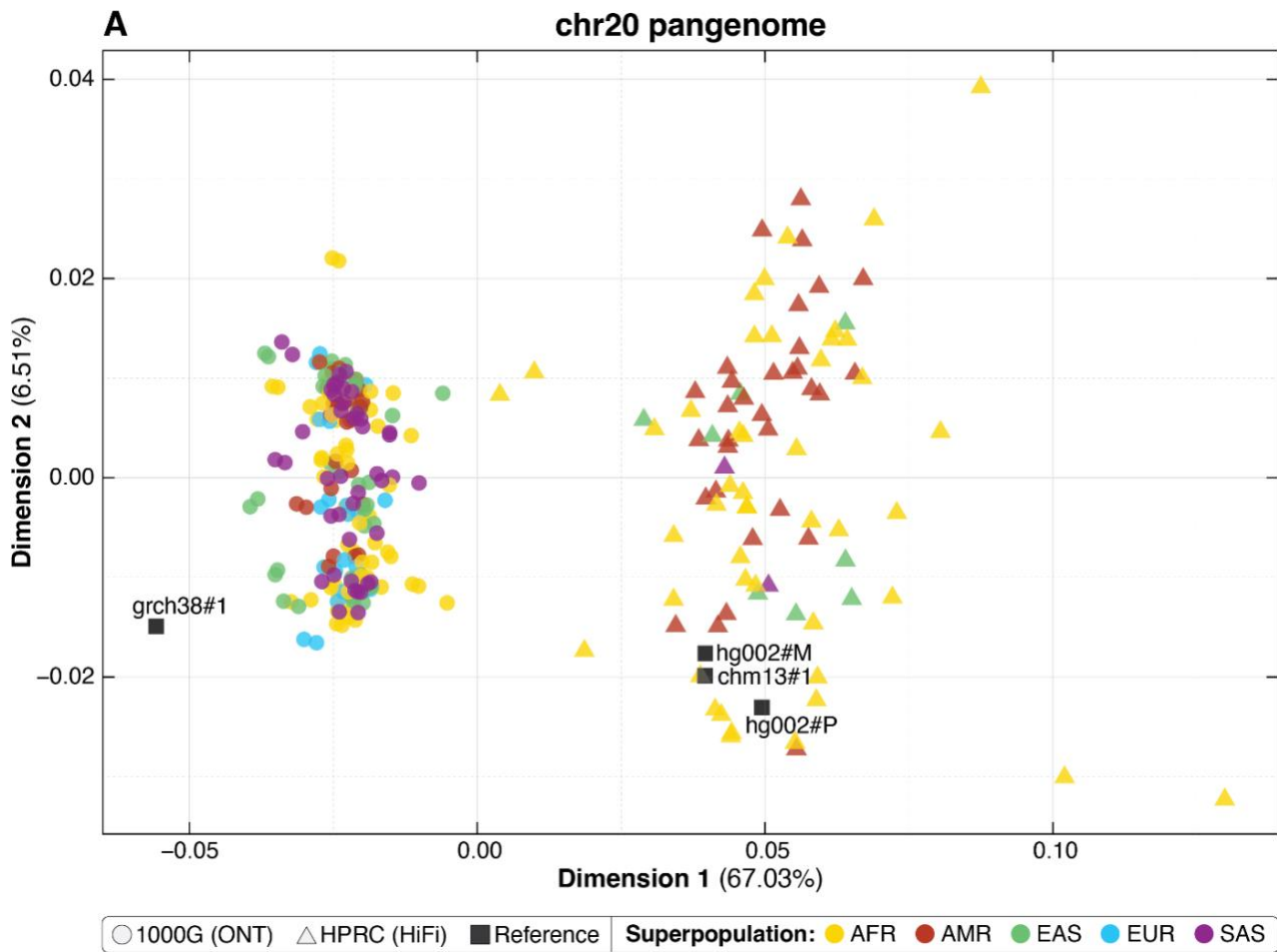


Figure S6. Evaluation of L1HS elements in the first 100 assemblies.

Comparison of the number of L1HS in the major populations in the 100 samples (standard boxplots) against the number identified in phased haplotypes from HG002 and HG005 from GIAB and the haploid CHM13 T2T assembly.

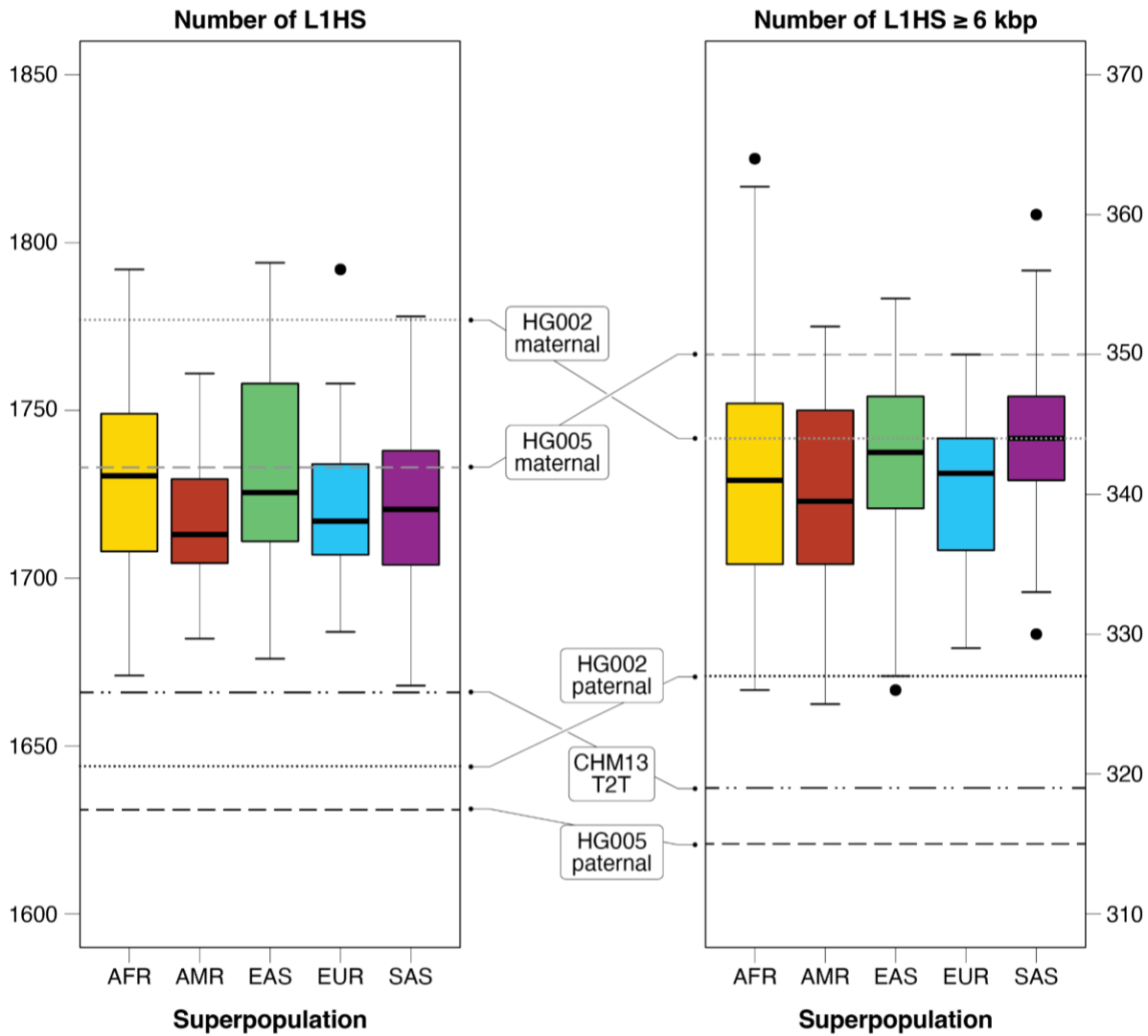


Figure S7. Evaluation of per-sample insertions and deletions by type, chromosome, and SV caller.

The number of insertion and deletion SVs was evaluated by chromosome for each of the five SV callers across all 100 samples.

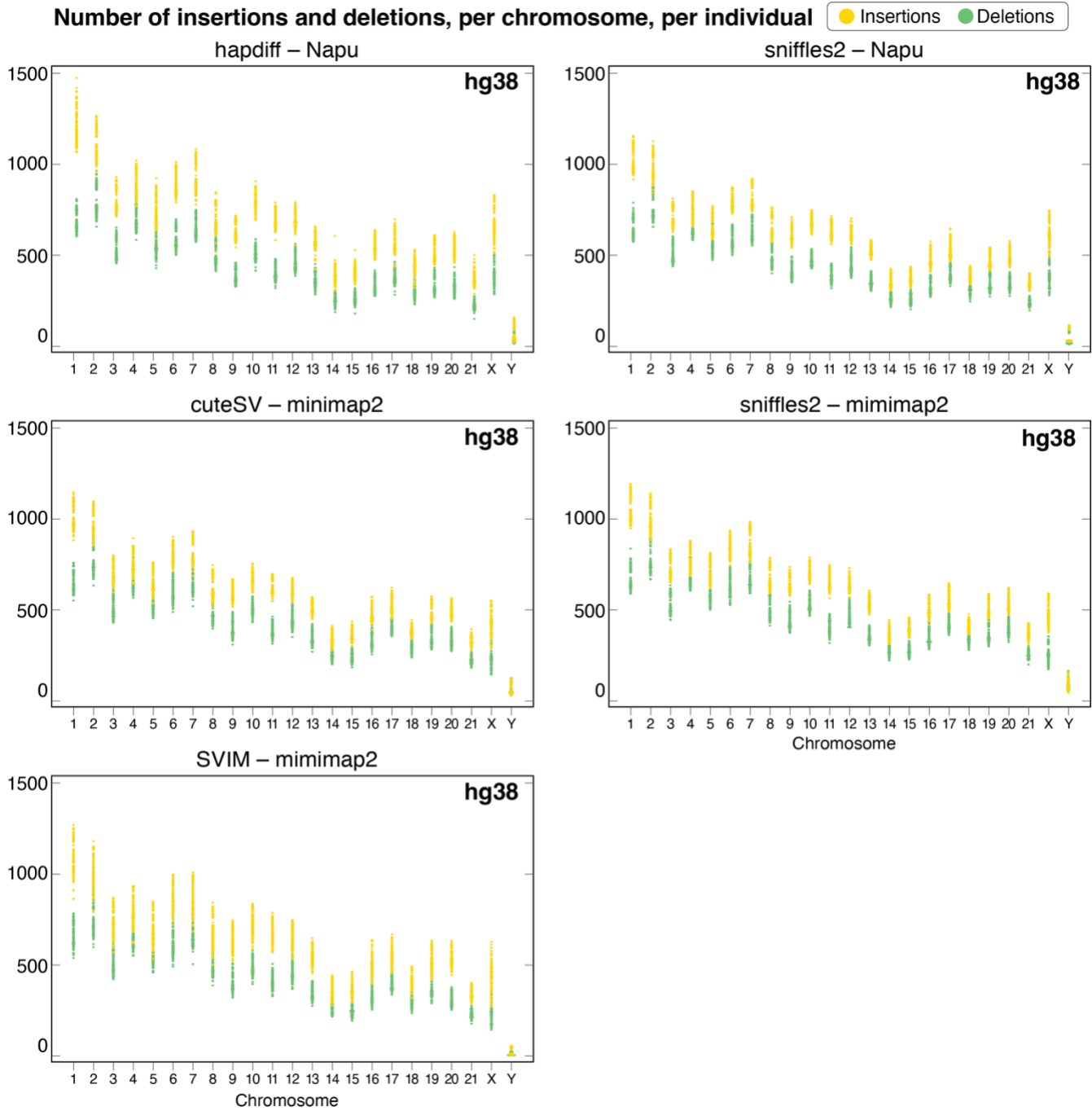


Figure S8. Distribution of SV events genome-wide, all populations.



Figure S9. Concordance of SVs by caller and evaluation of joint SV calls.

A,C. Concordance of SV calls for all callers (A) and for only hapdiff (C) for insertion and deletion events. **B.** Number of SVs per individual called by at least 1, 2, 3, 4 and 5 (all) callers. Based on Jasmine merging of all 5 SV callers per sample (cuteSV–minimap2, Sniffles2–minimap2, SVIM–minimap2, hapdiff–Napu, Sniffles2–minimap2). If an SV was called by at least one caller (in other words, called at all by any caller), it has a minimum support of 1. If an SV was called in an individual in at least 2 callers, it has a minimum support of 2, etc. 5 means that all 5 callers agree on the SV. We see the same expected distribution of AFR samples having more SVs in each support threshold.

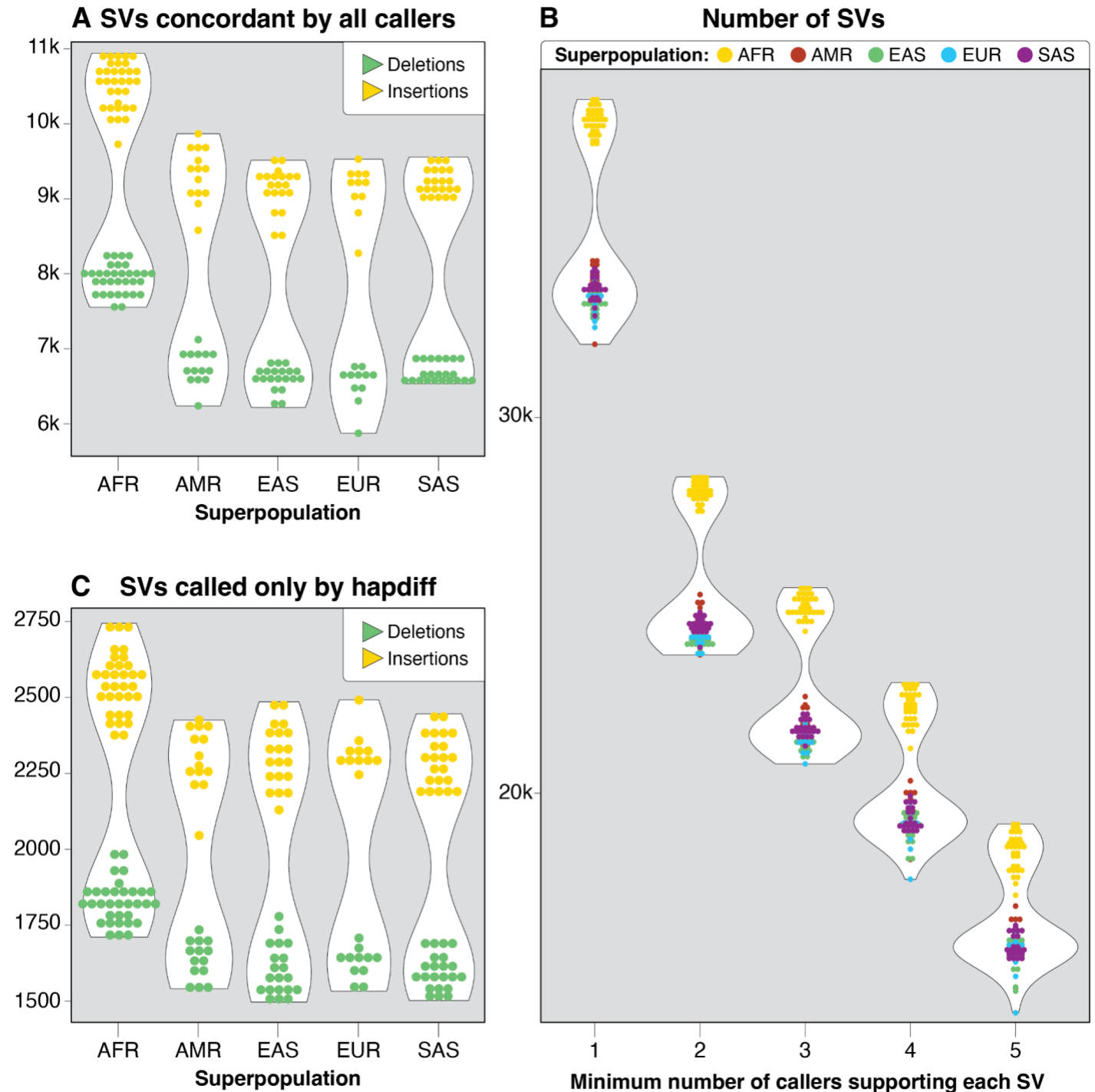


Figure S11. Evaluating the functional impact of structural variants.

A. Variant counts in the 65 samples common to both the 1000G-ONT and MAGE datasets (1 indicates heterozygous variants and 2 indicates homozygous variants). **B.** Relationship between the best-fit slope (β) derived from OLS regression and gene-level p-values. “All” refers to the use of identified SVs in selected samples for the eQTL analysis. “Novel” indicates the eQTL analysis conducted with SVs that were not reported in the previous long-read SV dataset of 31 samples by Kirsche *et al.* **C.** Integrative Genomics Viewer (IGV) screenshot of a 1235 bp deletion upstream of the 5' TSS of the TNFSF13 gene. **D.** Distribution of genotypes and gene expression values in the 65 samples for the TNFSF13-associated deletion, along with the Benjamini-Hochberg corrected p-value. We note the p-value reported by Kirsche *et al.* is 0.045, largely due to the larger number of samples considered after short read genotyping in GTEx. **E.** IGV screenshot of a 96 bp deletion downstream of the IFFO2 gene. **F.** Distribution of genotypes and gene expression values in the 65 samples for the IFFO2-associated deletion, along with the Benjamini-Hochberg corrected p-value.

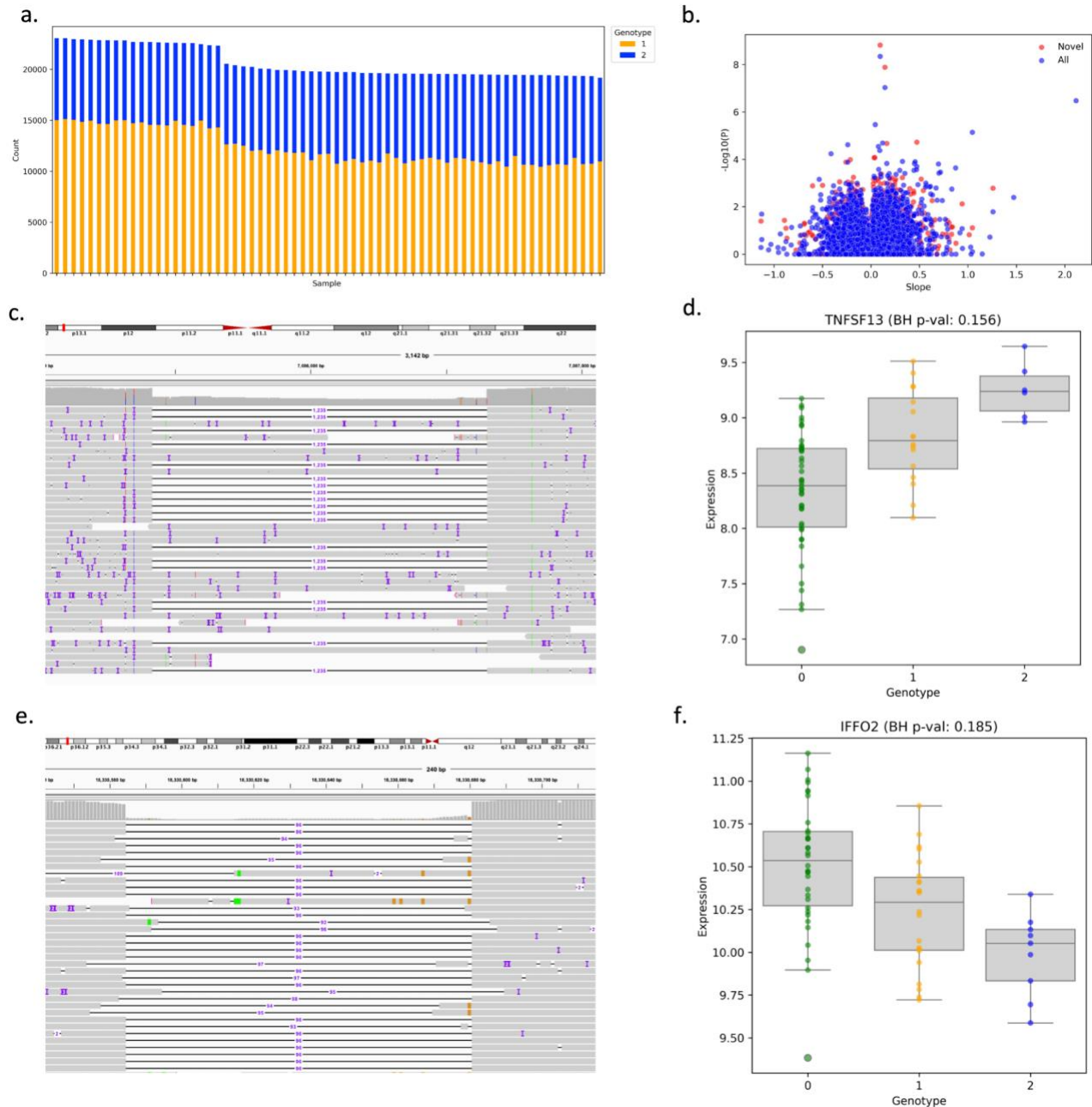


Figure S12. Evaluation of SVs in exons of medically relevant genes.

A. Number of samples harboring each INS/DEL intersecting an OMIM exon. **B.** Ideogram of where each SV that intersects with an OMIM exon is located in the GRCh38 genome

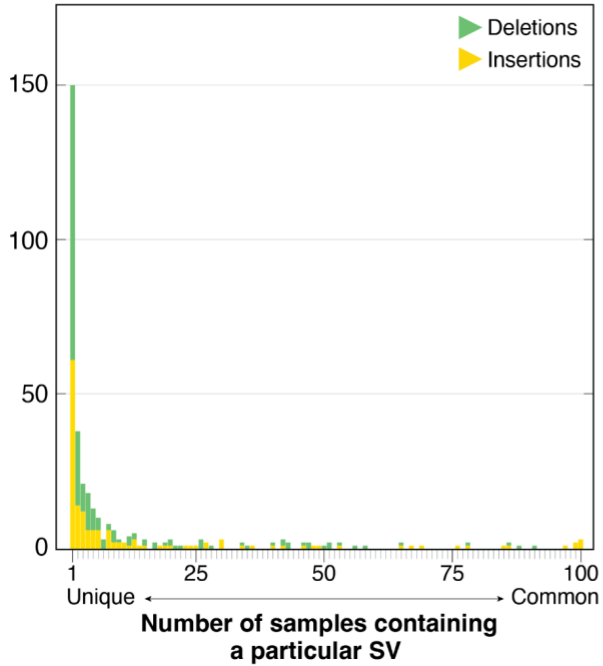
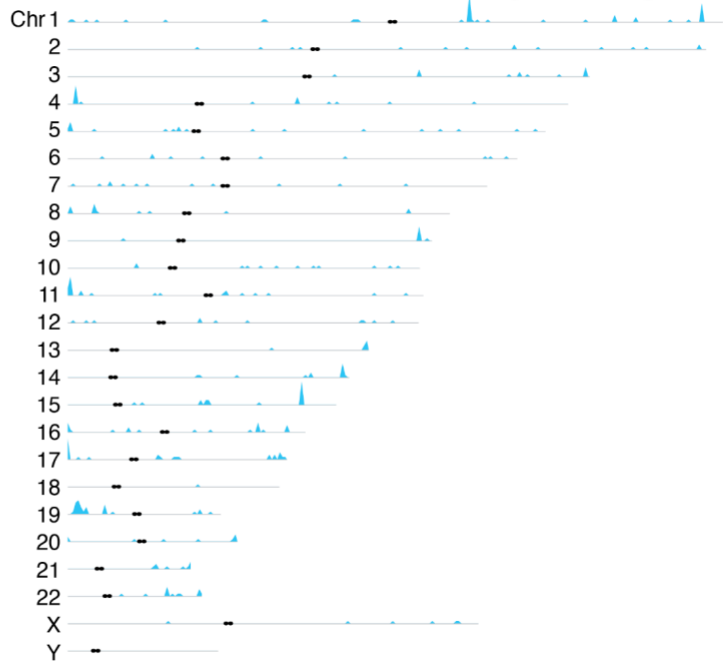
A Number of SVs in medically relevant genes**B Locations of exonic SVs in medically relevant genes**

Figure S13. IGV view of a previously described deletion that includes *HBM*, *HBA2*, *HBA1*, *HBQ1*.

A 19,304-bp deletion (NC_000016.10:g.165401_184701del) that includes *HBA1* and *HBA2* in HG01812 (Dia Chinese/EAS) and HG00728 (Southern Han Chinese/EAS). This deletion is commonly referred to as the Southeast Asian deletion (--SEA) and is associated with alpha-thalassemia (MIM: 604131).

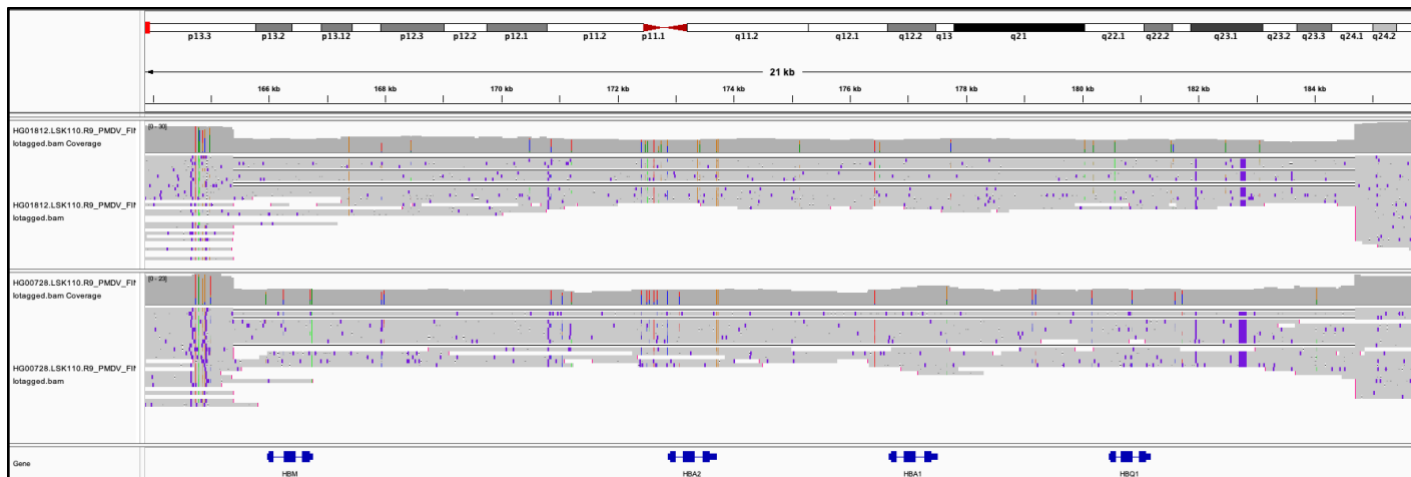
HG01812

Figure S14. Evaluation of X-linked SVs in 46,XY individuals.

A. Screenshot of alignments and assemblies for an approximately 141-bp insertion in *RPGR* in GM18865. The top two tracks depict Coverage and Alignments. Track 3 and 4 show assembly-based calls derived from Shasta-Hapdup assemblies with 146-bp insertion on one haplotype and 141-bp insertion on the other. The bottom track depicts Flye assembly with a 141-bp insertion. **B.** Screenshot of short-read data from GM18865 and LRS data showing that the 141-bp insertion is not apparent in the short-read data.

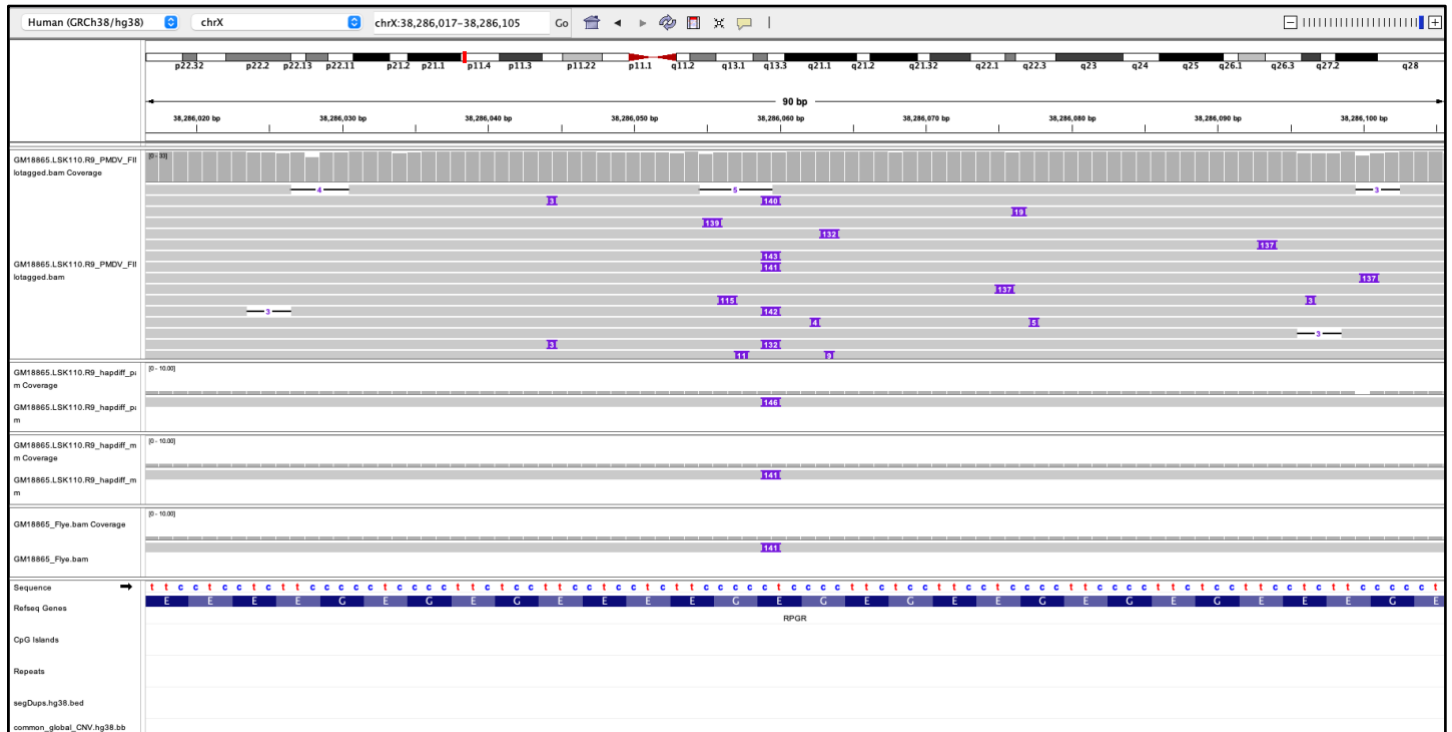
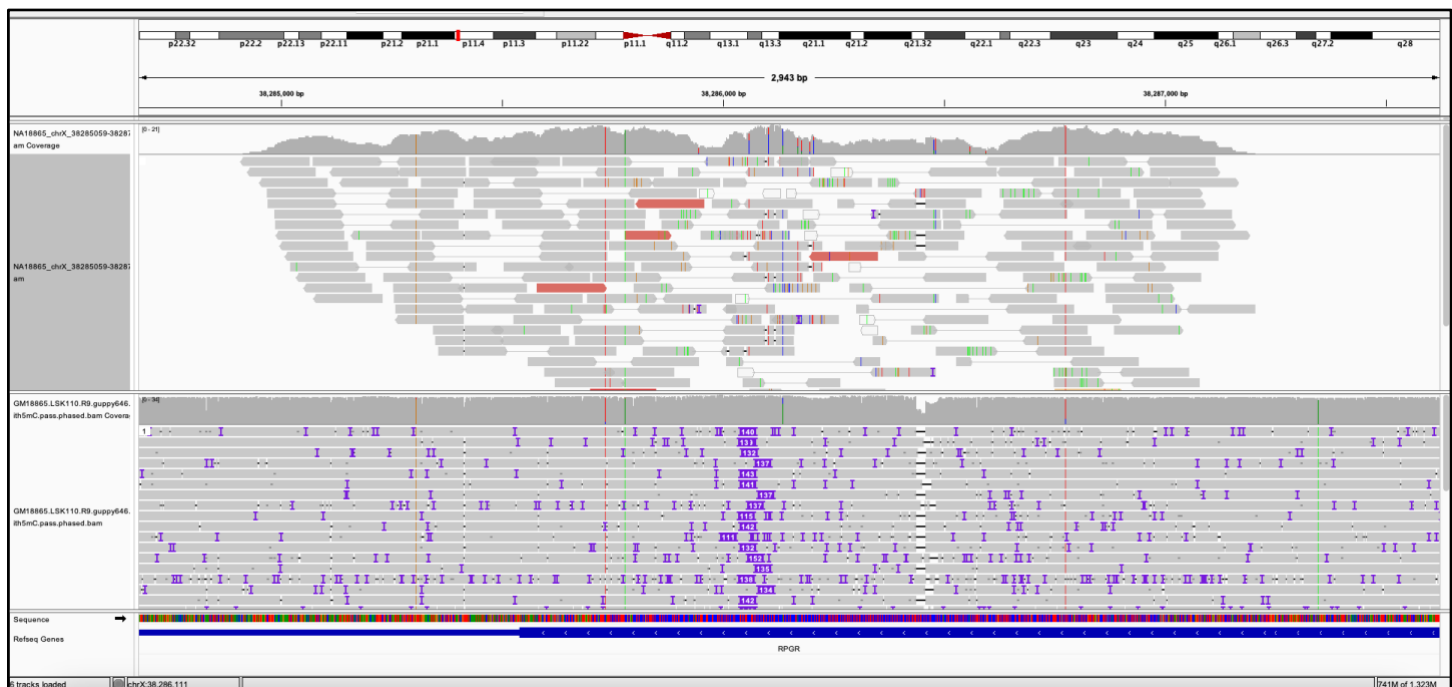
A**B**

Figure S15. Phased IGV screenshot depicting long-read alignments involving two pharmacogene hybrid star alleles.

Long-read alignment across CYP2B6 and CYP2B7 for GM18871 from an individual from the Yoruba in Ibadan (Nigeria) who has the CYP2B6*18/*29 diplotype. Short-read alignments are included for comparison.

CYP2B6*29 is a hybrid deletion allele with a CYP2B7-derived portion (across exons 1–4) and a CYP2B6-derived portion (covering exons 5–9). Read alignment results in reads aligned to either the gene (CYP2B6) or the pseudogene (CYP2B7), resulting in portions with numerous spurious SNVs.

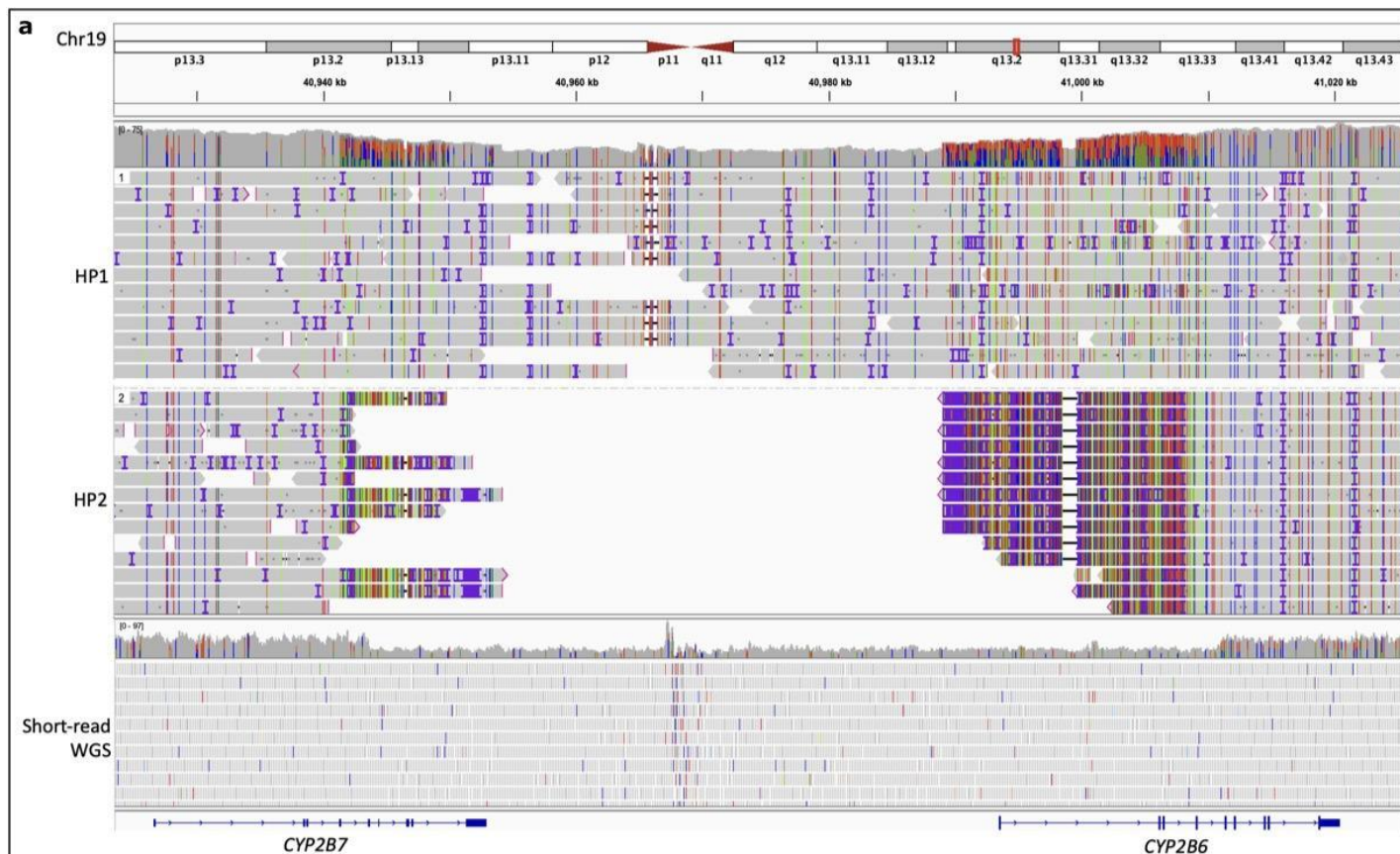
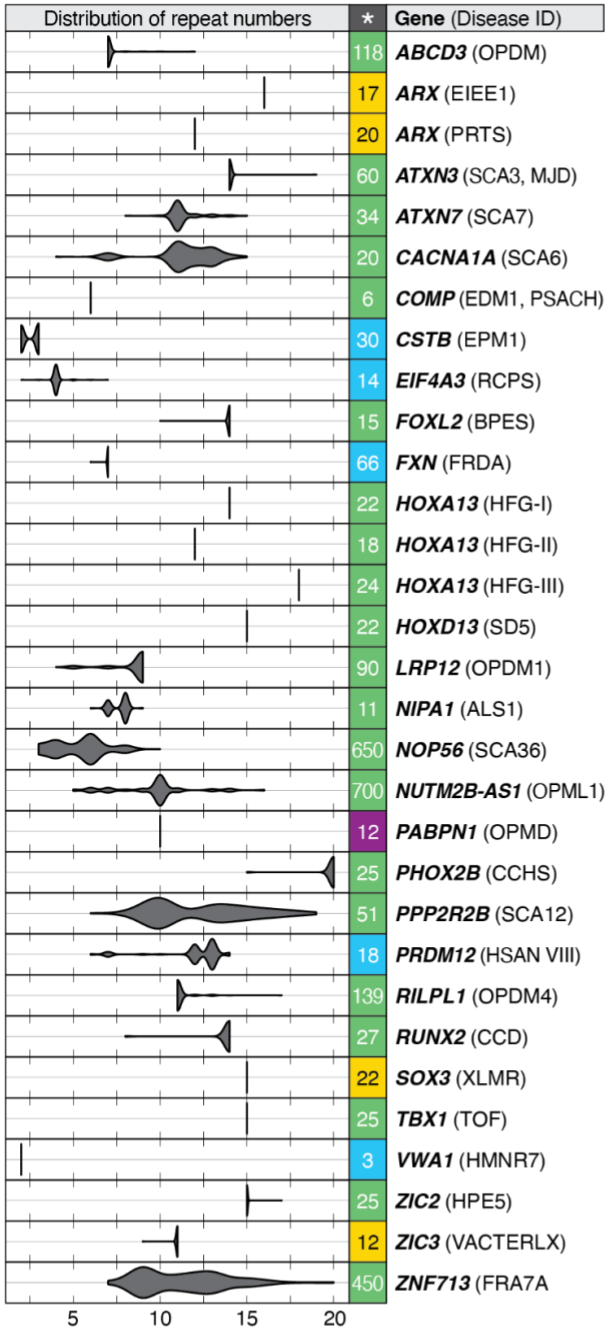


Figure S16. Repeat expansion plots for 66 disease-associated loci.

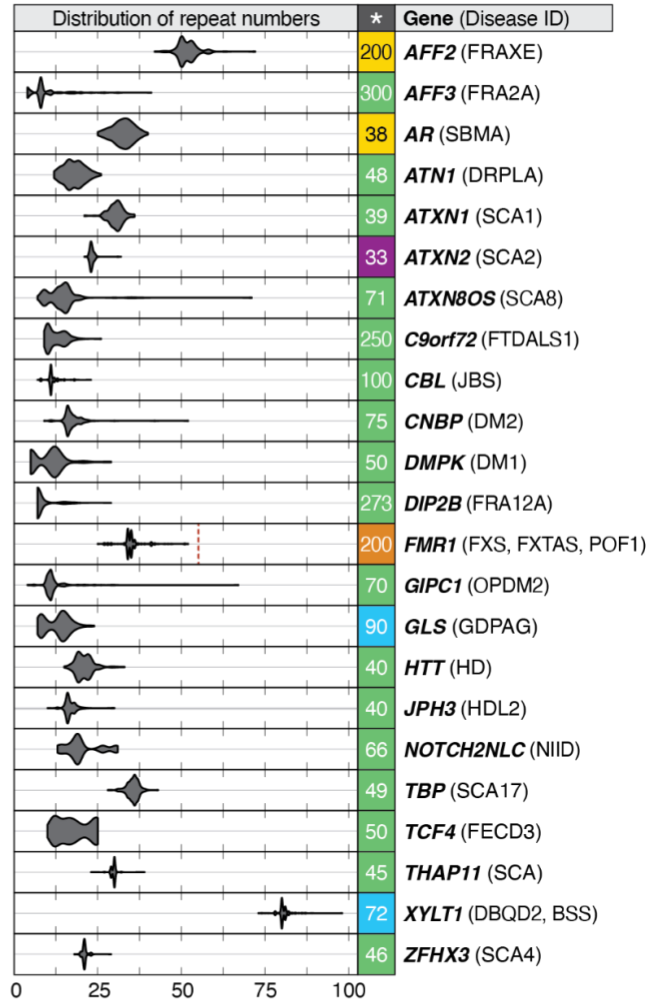
Violin plots for 66 disease-associated repeat expansion loci listed at STRchive:

<https://github.com/hdashnow/STRchive>. Motif counts were genotyped with vamos and plotted with R.

Simple repeat units

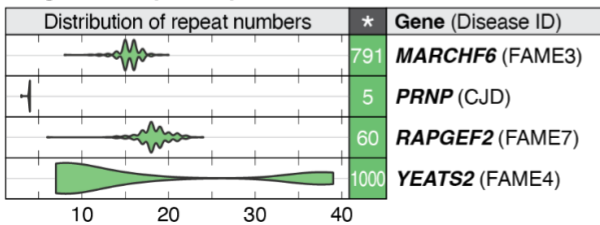


Simple repeat units

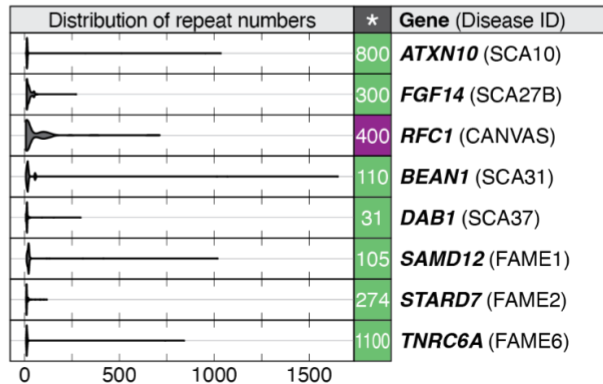


Inheritance pattern: AD AD/AR AR XR XD

Large or complex repeat units



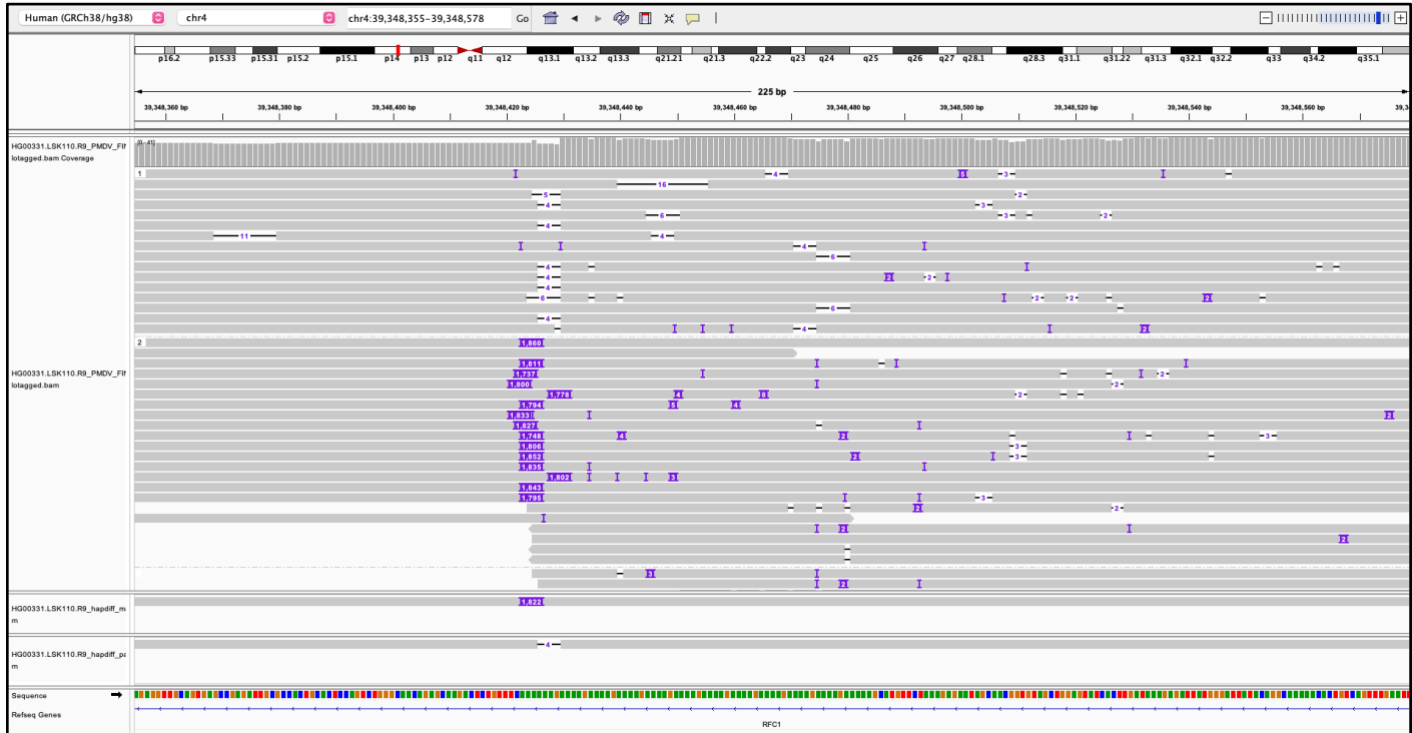
Large or complex repeat units



HG01122



HG00331



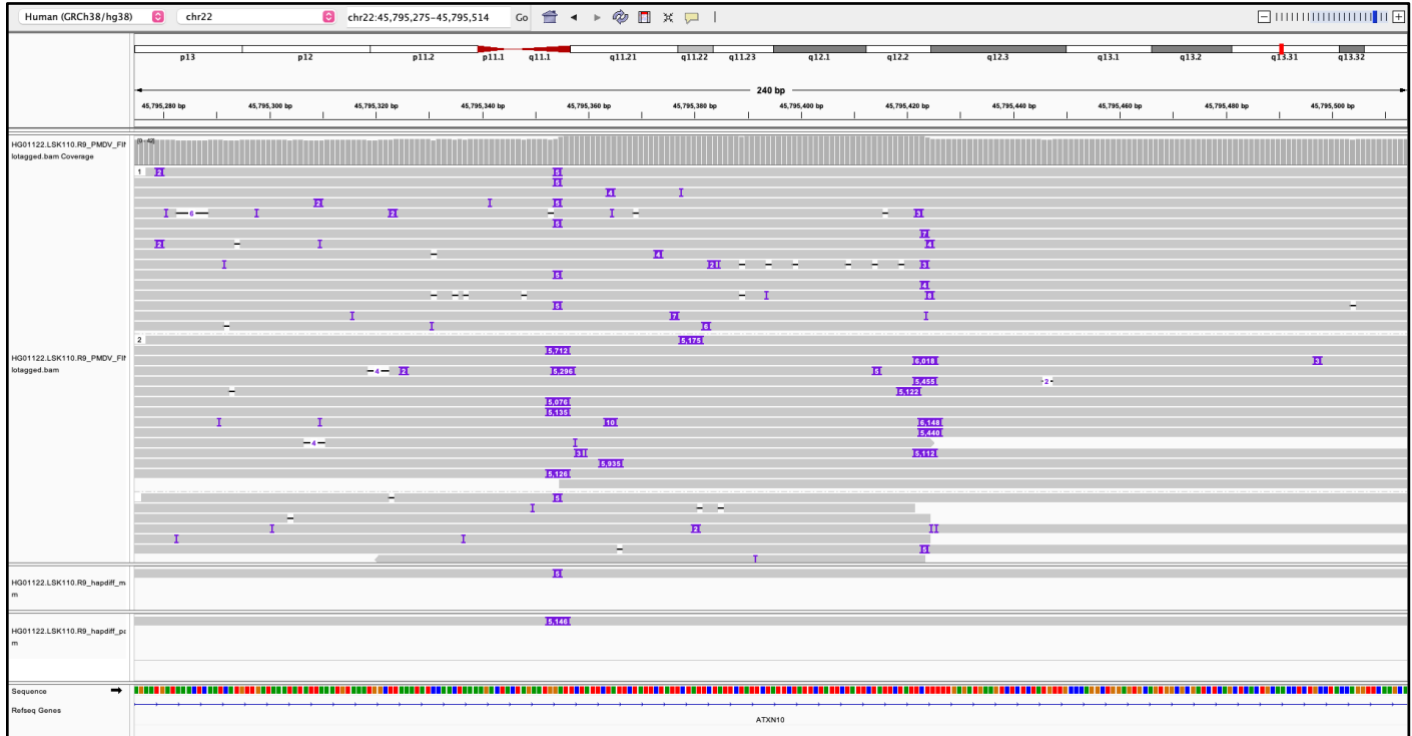
HG01862



Figure S18. IGV screenshots of *ATXN10* repeat expansions.

IGV screenshots for the three samples at the SCA31-associated locus at *ATXN10* with over 250 motifs. The PMDV haplotagged alignment and the hapdiff assemblies from the NAPU pipeline for each sample are shown. The hapdiff assembly files were used for genotyping with *vamos*.

HG01122



HG02252



HG02345

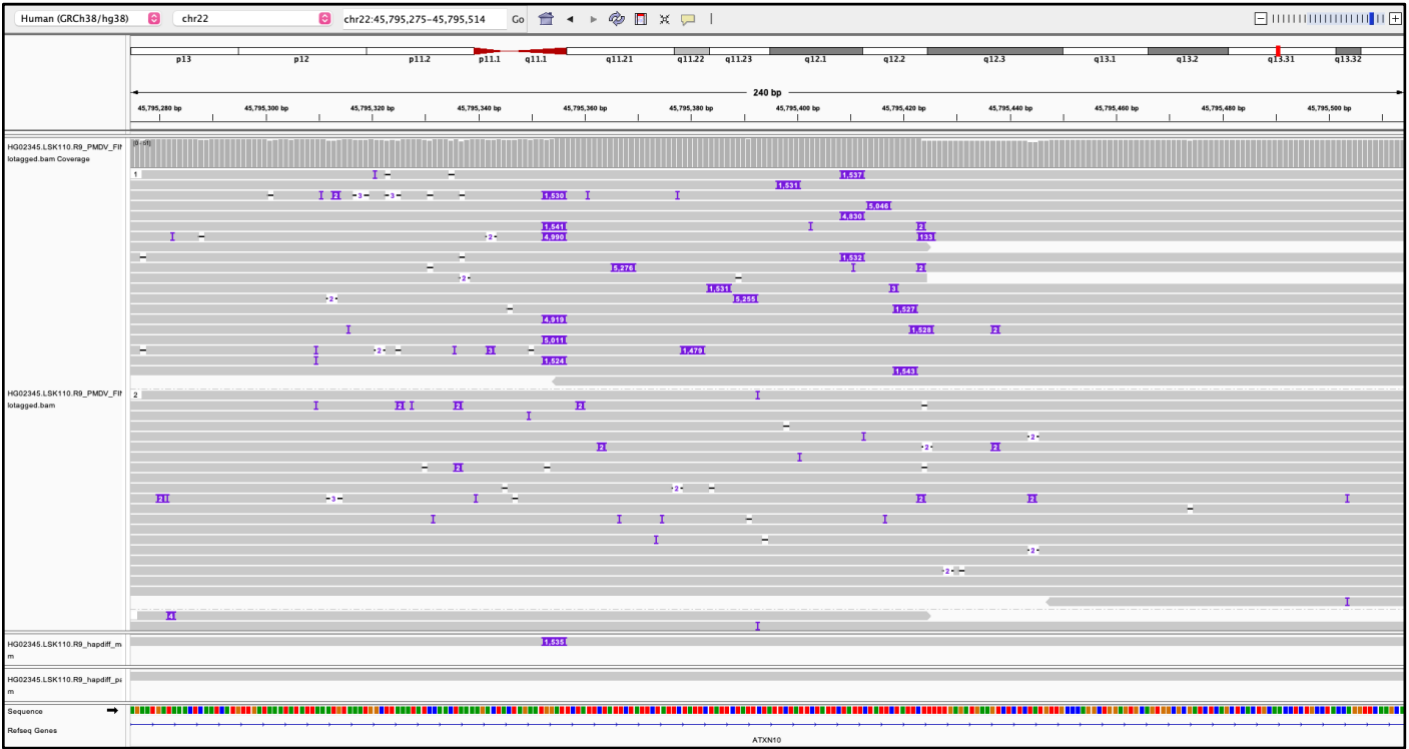


Figure S19. IGV screenshots of repeat expansion within *FGF14*.

IGV screenshot for the sample at the SCA27B-associated locus at *FGF14* with over 250 motifs. The PMDV haplotagged alignment and the hapdiff assemblies from the NAPU pipeline for each sample are shown. The hapdiff assembly files were used for genotyping with *vamos*.

HG01501



Figure S20. Principal component analysis using methylation.

The average methylation frequency for 27,050 CpG islands for 76 samples was used for performing PCA. One 46,XX sample (GM18864) clusters with the 46,XY samples.

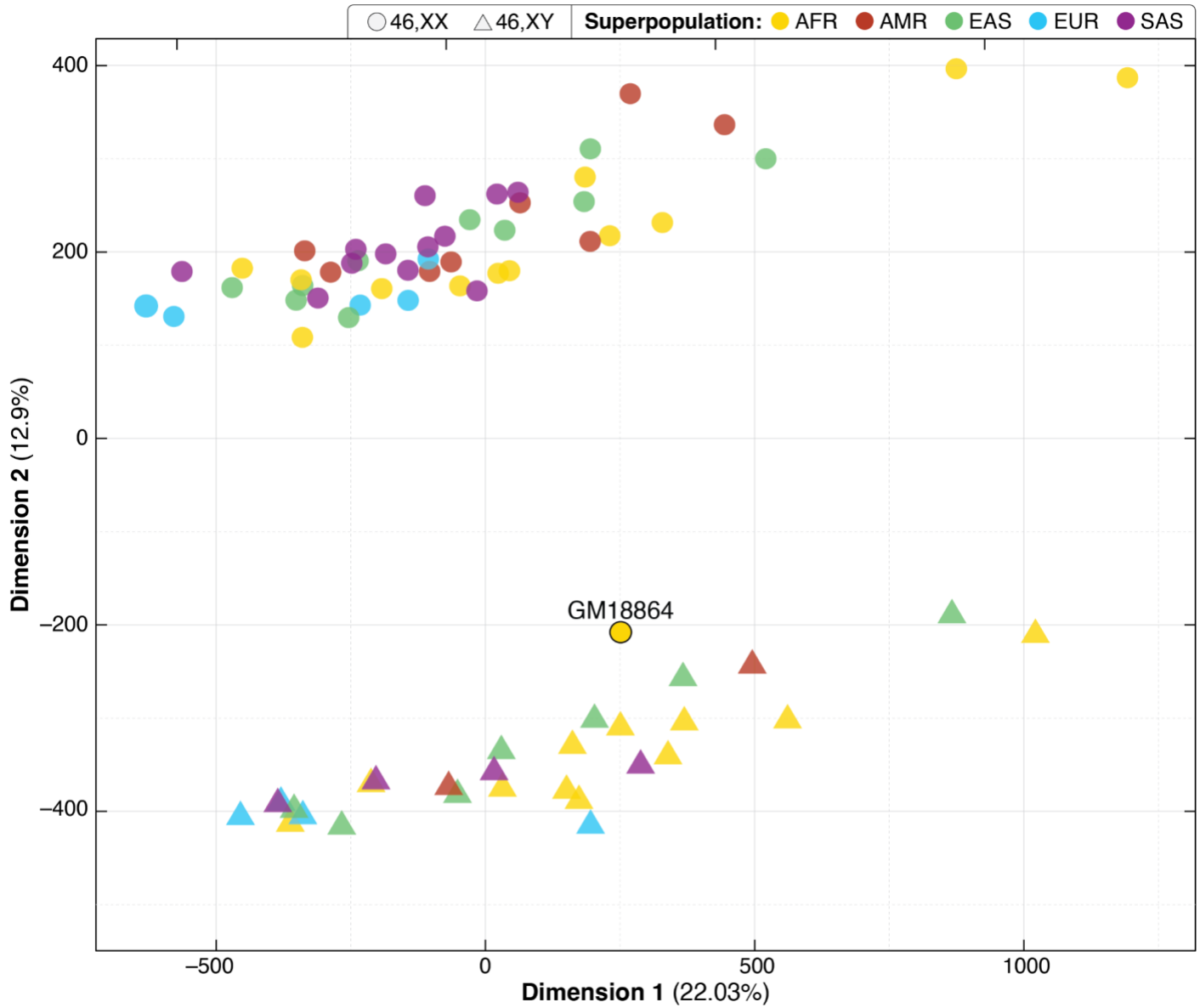


Figure S21. Evaluating methylation differences at *SNURF-SNRPN*.

A. Gain of methylation was observed in GM19473 (bottom), where both haplotypes are mostly methylated (red). HG03069 (top) is used as a control. **B.** Loss of methylation is seen in HP1 of HG00525 (top). HG04216 (bottom) is used as a control.

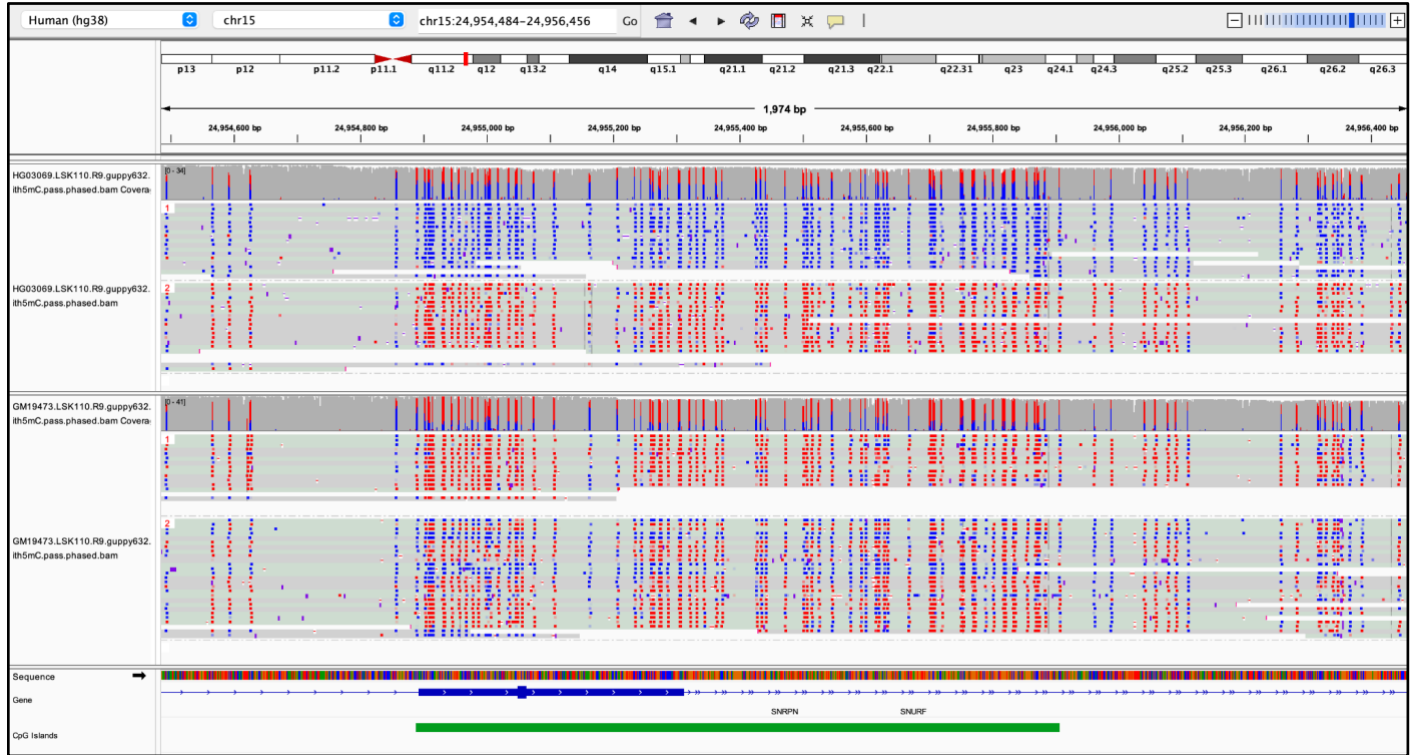
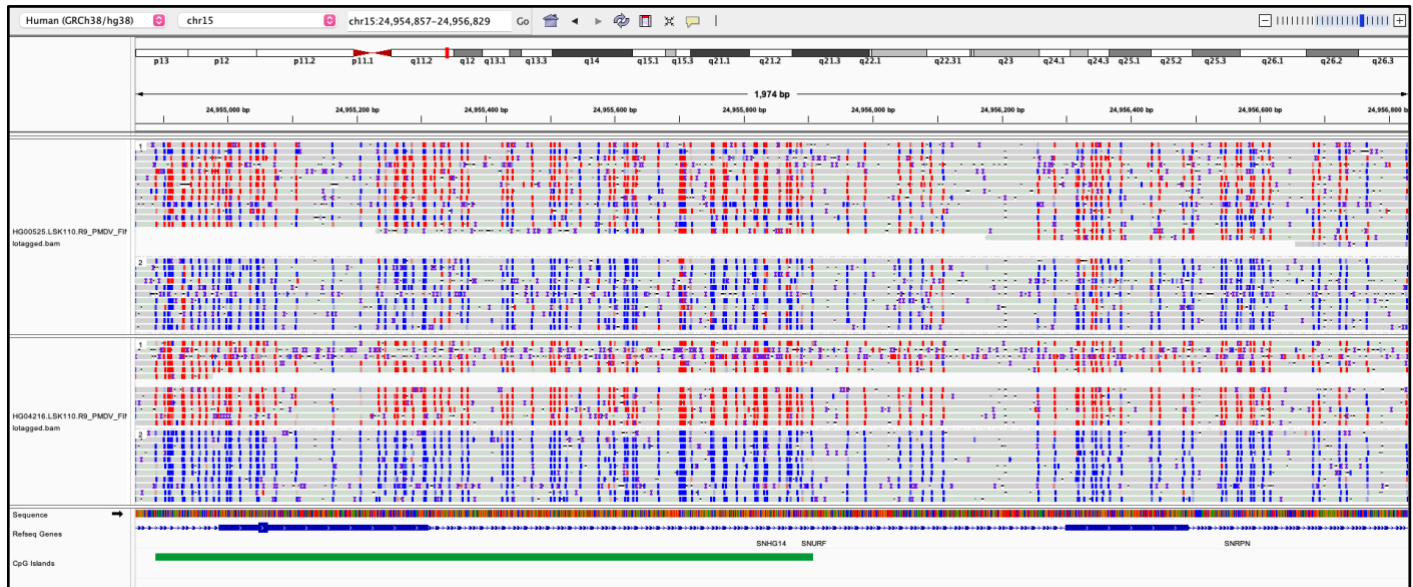
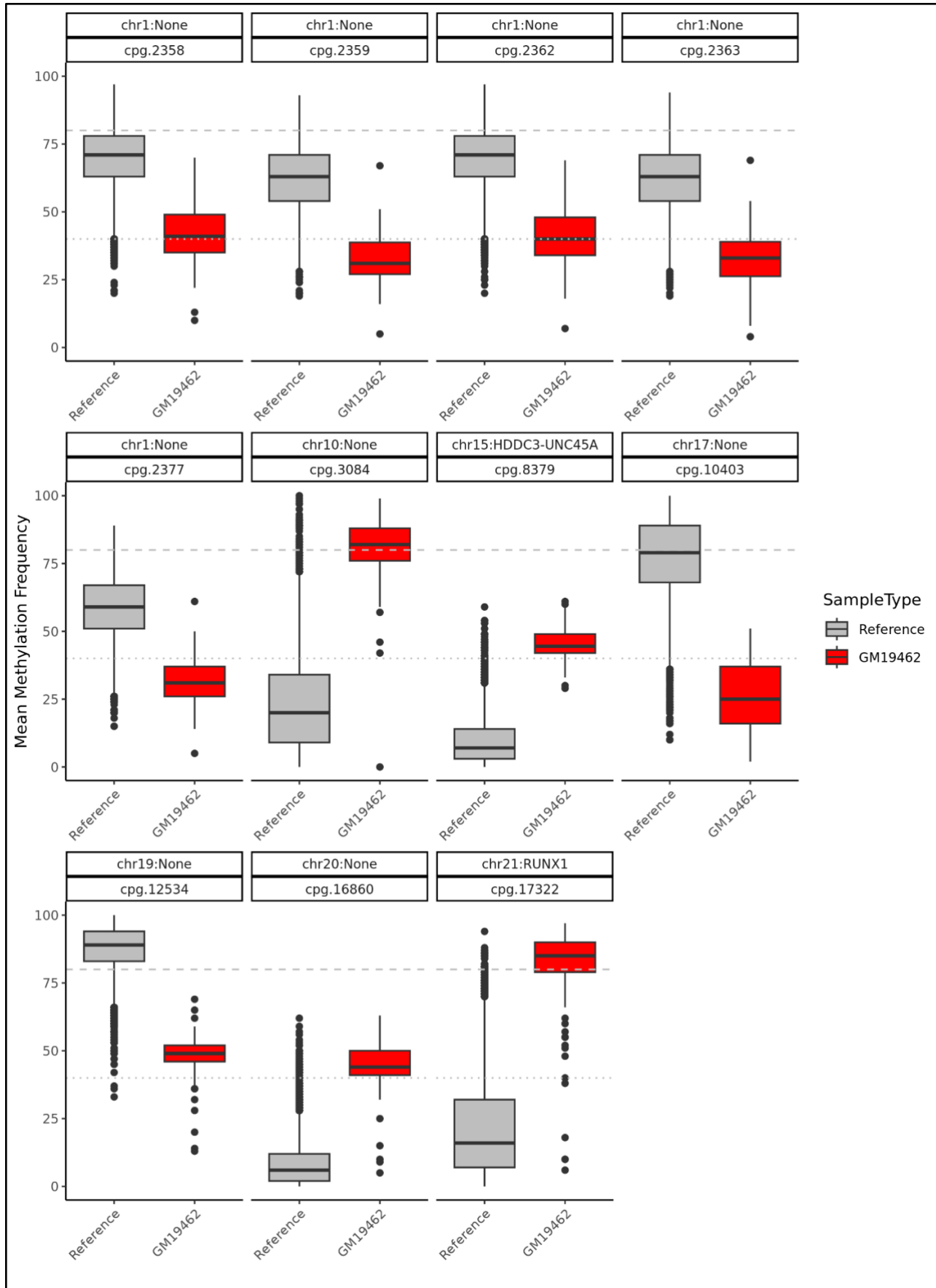
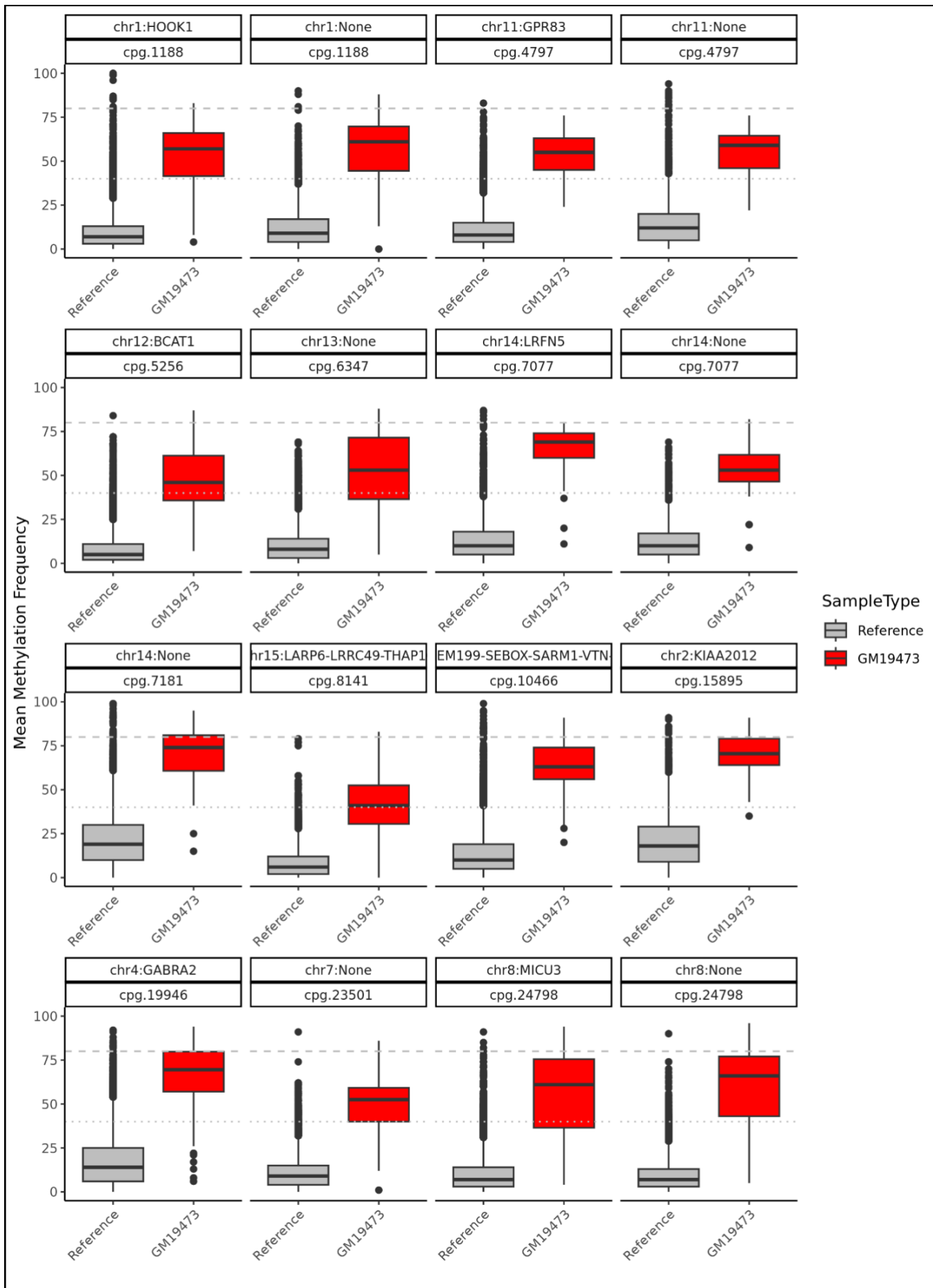
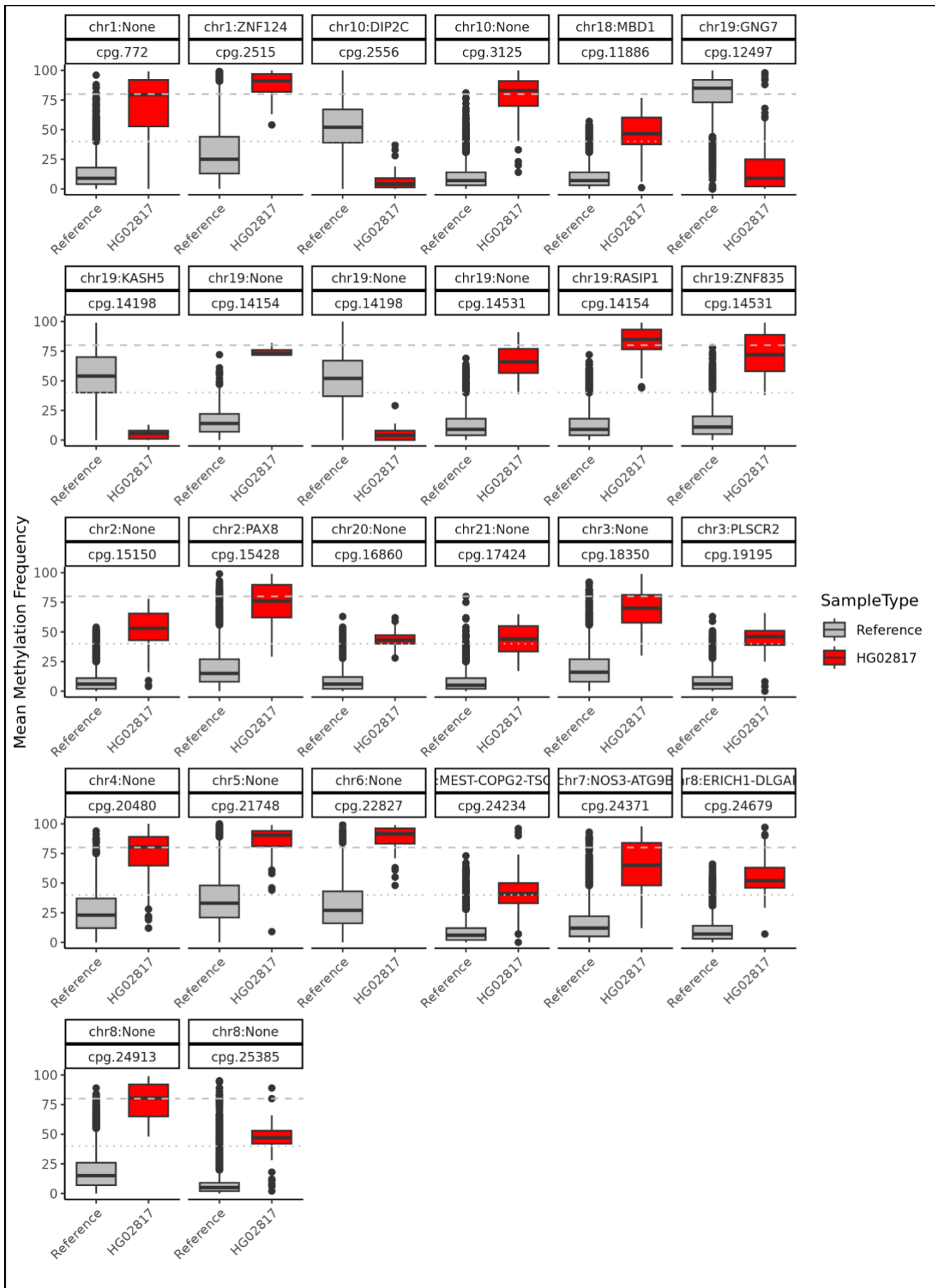
A**B**

Figure S22. Output from MeOW showing DMRs within 3 samples that have 10 or more DMRs.







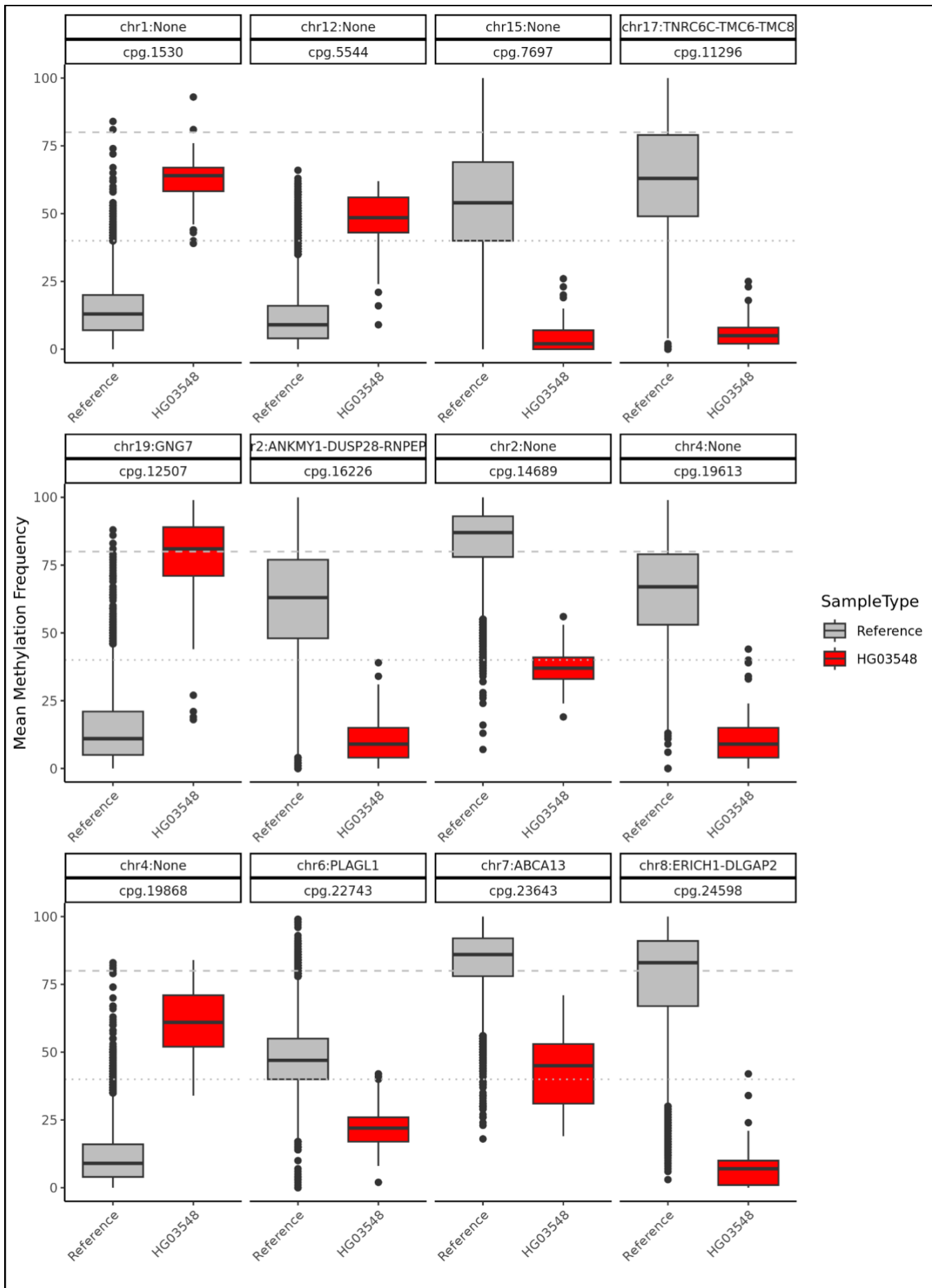


Figure S23. Unique DMRs are associated with nearby changes in gene expression.

Expression Z-scores thresholds from RNA-sequencing data for 15 AFGR samples for 85 genes in proximity (10kbp) of DMRs identified with MeOW versus log odds ratios across all sample-gene pairs to identify expression outliers.

